# A VOXEL-BASED MONTE CARLO RADIOTHERAPY SIMULATOR

K. Bliznakova, Z. Kolitsi and N. Pallikarakis

Department of Medical Physics, School of Medicine, University of Patras, 26500, Rio, Patras, GREECE

nipa@bme.med.upatras.gr

**Abstract: This paper presents a voxel-based Monte Carlo radiotherapy simulator. This simulator is an evolution of our previously developed radiotherapy simulator MCRTS that has been validated in a number of experiments related to general and specific radiotherapy applications. Further on, we have extended this simulator to include simulation of irradiation transport through patient specific data. For this purpose, a new module, called Voxel-based Simulation Module (VSM) has been introduced in the MCRTS. This new development includes adaptation of methods for irradiation transport through simple phantoms, as well as the design and the implementation of new modules that facilitate the use of patient data. The new code was tested and verified in terms of accuracy of dose calculation against data obtained from the MCRTS with phantoms, composed of simple geometrical primitives.**

## Introduction

The main goal of the recent radiotherapy is to deliver high and uniform dose to the target volume while sparing the surrounding healthy tissue [1]. The accuracy of dose calculation in a treatment planning system is therefore a critical issue. Among many algorithms developed over the last years, those based on Monte Carlo (MC) proved to be the most accurate technique used for dose calculations. These techniques provide detailed description of the radiation transport in the absorber therefore offer accurate 3D dose information. Tumor volumes are well delineated using 2D or 3D imaging techniques. Computed tomographic (CT) simulation has been widely adopted imaging technique, since it owns many advantages in accuracy, preparation of complex treatment plans and 3D gross tumour volume visualization.

We have recently reported a Monte Carlo Radiotherapy Simulator (MCRTS) [2] that can simulate radiation transport through a user defined system, including source, collimators, shielding absorbers, phantom and detector. This software has been extensively evaluated against data produced by other MC codes as well as experimental data [2, 3]. One limitation of this simulator was that it was not adjusted for simulations through voxel-based (tomographic) phantoms. The present work addresses research needs for simulation of radiation transport through tomographic phantoms and even more complex phantoms, i.e. combinations of tomographic phantoms and objects, defined by means of solid geometry. Such phantoms are designed for the evaluation of complex and novel radiation therapy techniques [3], to perform advanced MC simulation through the newly developed 3D breast model [4] and portal imaging studies [5].

More specifically, the objective of this work has been to develop applications for particle transport simulation through patient specific data. For this purpose a new module, called Voxel-based Simulation Module (VSM), intended for the particle transport simulation through voxel-based phantoms has been introduced in the MCRTS. Changes were introduced in the existing modules as well, in order to allow the use of CT patient data. New algorithms for particle transport through voxels were developed and implemented. They were subsequently tested extensively in terms of accuracy of dose calculation against data obtained from the MCRTS with phantoms, composed of simple geometrical primitives for various simple and complex geometries. These new features were evaluated in an application including modeling the spinal cord protection using rotational radiotherapy for treatment of a neck cancer [3].

## Materials and Methods

The voxel-based MCRTS is comprised of the following main modules: 1) phantom modeling, 2) geometry modeling, 3) beam modeling, 4) dose matrix specification, 5) irradiation transport through voxel primitives (VSM), 6) image formation modeling and 7) visualization facilities of the simulated geometry and simulated data. The new modules in this simulator compared to the previous version are the *phantom module* and the *VSM*.

*Phantom module.* The *phantom module* includes possibilities to load CT image patient data, to construct a 3D patient matrix and subsequently to correlate each voxel information to a corresponding material, characterized by the attenuation coefficients, the density and the mass. The user can assemble custom 3D patient matrices as well. Further more, for some specific applications, the phantom can be model as a synthesis of voxel and simple 3D primitives (complex phantoms). For the purposes of this verification study, the following phantoms were modeled.

*Homogeneous phantom.* Homogeneous water phantom ($\rho = 1$ gcm$^{-3}$) with dimensions shown in Figure


ISSN: 1727-1983 

1a was designed as a solid object. Subsequently, this solid object was mathematically transformed into a volume, comprised of a number of voxels (Figure 1b). This number depends on the chosen voxel resolution. For all the simulation experiments, carried out in this study, the voxel resolution was 1 $mm^3$.

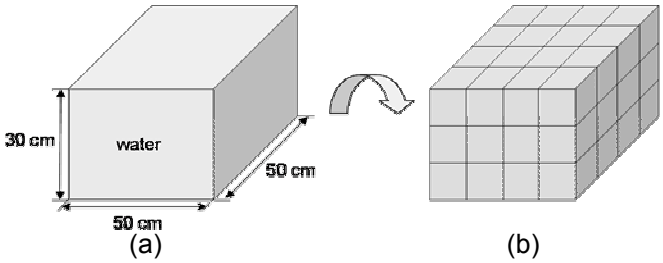


Figure 1: Homogeneous water phantom, defined as (a) solid geometry (geometrical primitives); (b) voxel-version of the same phantom.

*Heterogeneous phantom.* Inhomogeneity was simulated by means of an embedded bone slab ($\rho$ = 1.85 $gcm^{-3}$) of 10 cm thickness, placed at a depth of 10 cm in a water phantom with dimensions 50×50×30 $cm^3$ as shown in Figure 2. Voxel-based version of this phantom is created similarly to the previously described phantom.

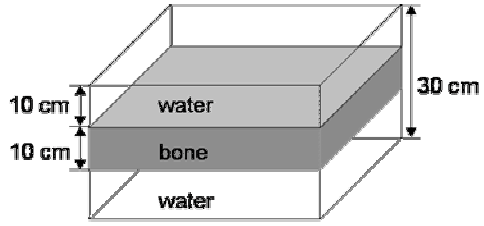


Figure 2: Heterogeneous phantom.

*Tomographic phantom.* Tomographic phantoms are constructed from CT patient data. One such phantom was composed of 30 CT images, taken from the National Library of Medicine's Visible Human Project® [6], each slide with dimension of 250 pixels in both directions (Figure 3a).

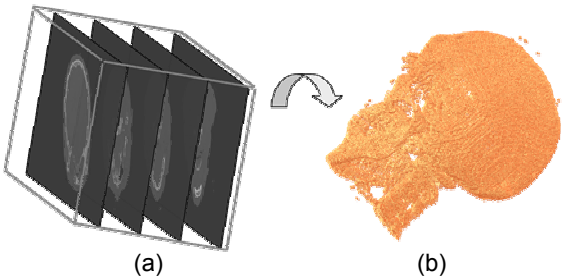


Figure 3: Tomographic phantom (a) patient specific data; (b) solid version of the tomographic phantom.

Pixel size was 1 mm, therefore the obtained tomographic phantom was 250×30×250 $mm^3$. For verification purposes, voxels that belong to this phantom were replaced by a cubic object with dimension of 1 mm (Figure 3b). The phantom was then subjected to a voxelization procedure. An optimization was applied to the composite mathematical phantom that aimed to decrease the number of objects in order to accelerate the simulation of radiation transport through them.

*Neck phantom.* The neck was modeled as a water cylinder, while the spinal cord was simulated as a cylinder with assigned interaction coefficients of the grey/white matter (Figure 4). The spinal cord was located in the center of the neck phantom.

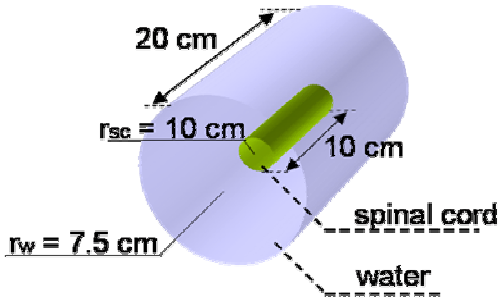


Figure 4: Neck phantom, containing the spinal cord as organ at risk (OAR), designed with solid-geometry objects.

The *VSM* module has been designed to facilitate the simulation transport through voxel-based and complex phantoms, since there are specific particle tracing algorithms applied to those two cases. The new particle subroutines calculate the particle position in the voxel matrix and consequently extract data for the voxels where the particles belong. These data are needed to calculate transport distances and interaction mechanisms. Smaller sub-steps, usually 1/10 of the voxel size are chosen to transport the particles through the voxels. The interaction mechanisms were entirely adapted from the High Energy Simulation Module (HESM) [2].

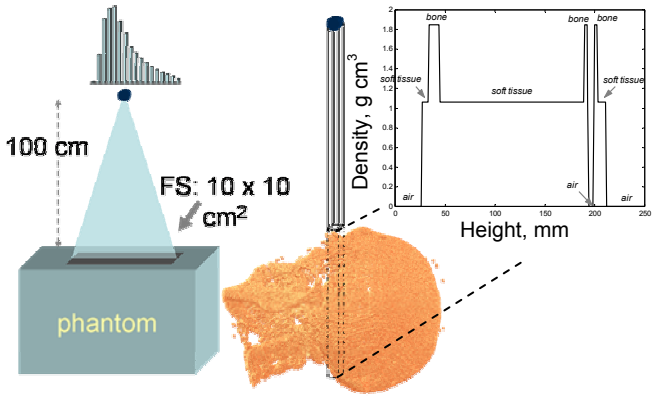


Figure 5: Irradiation geometries: a) fan beam, gantry at $0^0$; b) pencil beam, gantry at $0^0$.

Three *irradiation geometries* were simulated for the experimentations that are graphically depicted in Figure 5. In case of the tomographic phantom (Figure 5b), the pencil beam passes through the central part of the


ISSN: 1727-1983 

phantom, the density profile of which is shown in the insert of Figure 5b. Rotational therapy application with "omiotheta" beam modulator (OBM) is implemented using the geometry shown in Figure 5c. Briefly described, OBM is an absorber (in our case lead), which is a proportionally miniaturized copy of the organ at risk (OAR). During rotational therapy, it maintains the same position in relation to the OAR.

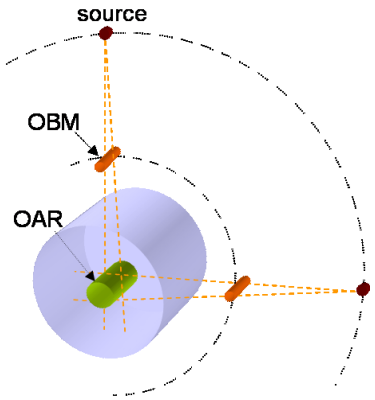


Figure 5c: Irradiation geometries for rotational therapy application.

## Results

*System validation* has involved comparison with data produced by the MCRTS, using phantoms composed from simple 3D geometrical primitives. For this purpose, various phantoms were modeled and subjected to radiotherapy simulation, using different irradiation geometries. A field size of $10\times10cm^2$ and source to surface distance 100 cm were used to estimate the initial photon fluence. Photon fluencies were selected in order to obtain overall average statistical uncertainty of less than 1%. Monoenergetic and polyenergetic beams were used for the simulations. Evaluated parameters included Central Depth Dose (CDD) and Percentage Depth Dose (PDD) curves, dose profiles and absorbed doses. They were evaluated in terms of accuracy of dose calculations. In case of CDD, dose distributions were normalized to the initial photon fluence ($\Phi_0$ / $cm^2$). For simplicity, the MC data obtained using simulation in phantoms defined with geometrical primitives (solid geometry) were labeled with OMC (object MC), while those obtained in voxel-based phantoms were labeled correspondingly with VMC (voxel MC).

*Experiment 1. Homogeneous phantom.*

This experiment was designed to verify the accuracy in the simulation of the transport of charged particles in a homogeneous voxel-based phantom. The two homogeneous water phantoms (solid and voxel-based) were subjected to photon fan beams with energies of 3MeV and 6MV. Ten runs, each comprised of $23*10^6$ photons per field size were simulated in both cases, in order to achieve the required statistical accuracy of the MC data. Dose matrix voxel size was $10\times10\times2$ $mm^3$.

The comparison between CDD curves and dose profiles for four different depths are shown in Figure 6a,b for the monoenergetic case, while Figure 6c shows the comparison between PDD curves for polyenergetic case. The highest discrepancy between the CDD curves is 3% in case of monoenergetic beam. The same discrepancy is registered for the dose profiles, while in case of polyenergetic beam this deviation is of order of 4%.

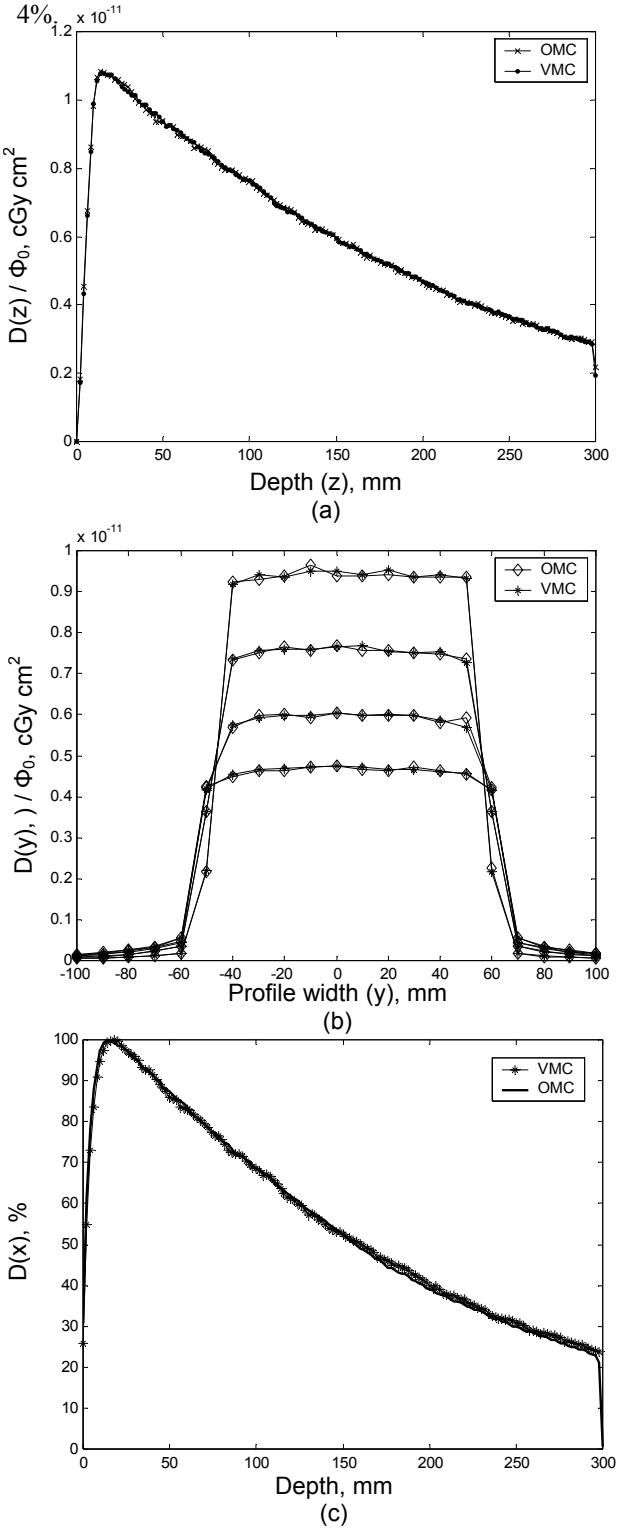


**Figure 6.** Comparison of simulated (a) CDD curves and (b) lateral dose profiles with the 3MeV beam incident on solid (OMC) and voxel-based (VMC) objects; (c) PDD comparison between simulated data for 6MV photon beam.


ISSN: 1727-1983 

*Experiment 2. Heterogeneous phantom.*

This experiment was designed to verify accuracy in the simulation of the transport of secondary charged particles in heterogeneous phantoms, at the inhomogeneity interface, where dose redistribution occurs. 2MeV and 6MV photon fan beams (Figure 5a) from a point source with uniform angle photon distribution were simulated using different initial photon fluence. Two voxel sizes were selected: i) 40×40×3 $mm^3$ and ii) 2×2×2 $mm^3$. The first voxel size was used in the experiment involving CDD comparison, while the second voxel resolution was used for dose profiles comparisons. Photon fluences are shown in the table. The CDD curves and dose profiles at three depths of 5, 15 and 22 cm are shown in comparison in Figures 7a,b in case of 2MeV, while Figure 7c shows the PDD result in case of 6MV photon beam.

| *Incident beam* | *Dose voxel size, $mm^3$* | *Photon fluence* | *Purpose* |
|---|---|---|---|
| 2MeV | 40×40×3 | $23\times10^6$ | CDD curve |
| 2MeV | 2×2×2 | $7\times10^8$ | profile distributions |
| 6MV | 10×10×2 | $23\times10^7$ | PDD curve |

Table: Photon fluence used for the heterogeneous experiments.

The results for monoenergetic case show maximal discrepancies of 5% observed at the inhomogeneous boundaries, while at the rest of the CDD curve the corresponding deviation is smaller than 2%. Similar results are shown for the profile comparison. In case of polyenergetic beam, the maximum deviation between the two CDD curves was observed at the inhomogeneity interface (17%), while for the rest of it, the deviation does not exceed 3%.

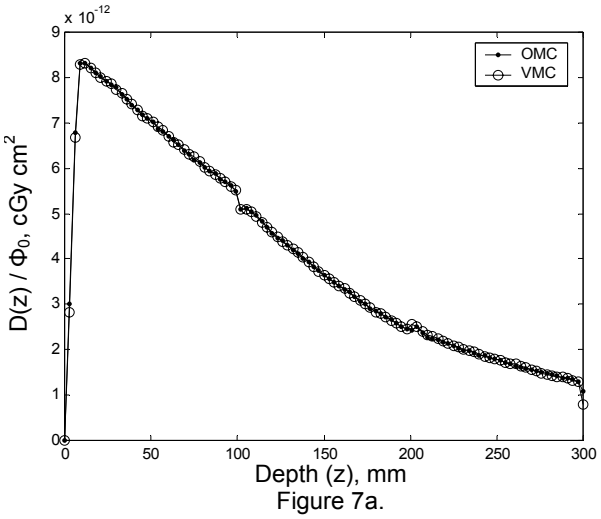


Figure 7a.

*Experiment 3. Tomographic phantom.*

This experiment was designed to test the accuracy of modeled particle transport through patient specific data. The head tomographic phantom and its solid version were subjected to pencil beams with energies ranging in the interval 0.2 to 3 MeV (Figure 5b). 30 runs per incident energy were simulated. Each run comprised of

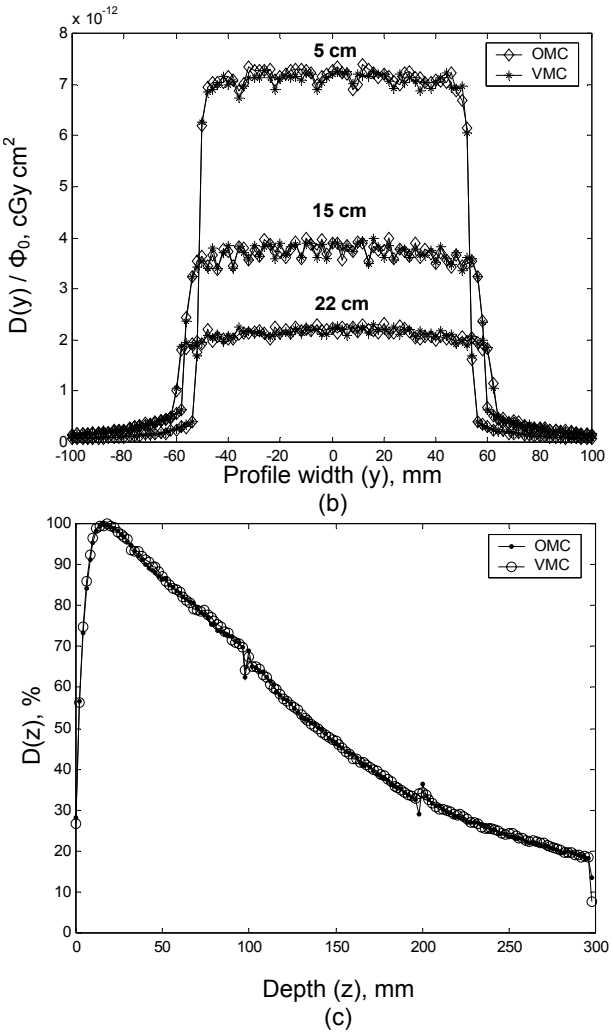


Figure 7: Comparison of simulated (a) CDD curves and (b) lateral dose profiles with the 2MeV beam incident on solid (OMC) and voxel-based (VMC) objects; (c) PDD comparison between simulated data for 6MV photon beam.

$10^4$ incident photons. Dose matrix resolution was 2×2×2 $mm^3$. CDD curves for the two of energies and absorbed dose in the central volume defined as 2×2×250 $mm^3$ were evaluated and comparison is presented in Figure 8 a,b,c. The largest deviation between the absorbed doses (Figure 8a) in the two phantoms was 2%, registered at higher incident energies. Bigger deviations are observed, while comparing the CDD curves.

*Experiment 4. Rotational therapy application.*

The new VSM has been verified in a specific application included rotational therapy with OBM. This specific application includes modeling of the spinal cord protection using OBM and rotational radiotherapy for the treatment of a neck cancer. This application is a demonstration of simulation of complex geometries that requires combination of ray tracing techniques through voxelised and solid defined volumes. The solid geometry phantom and its voxel-based version (Figure 4) and the irradiation geometry shown in Figure 4) and the irradiation geometry shown in Figure 5c were used.


ISSN: 1727-1983 

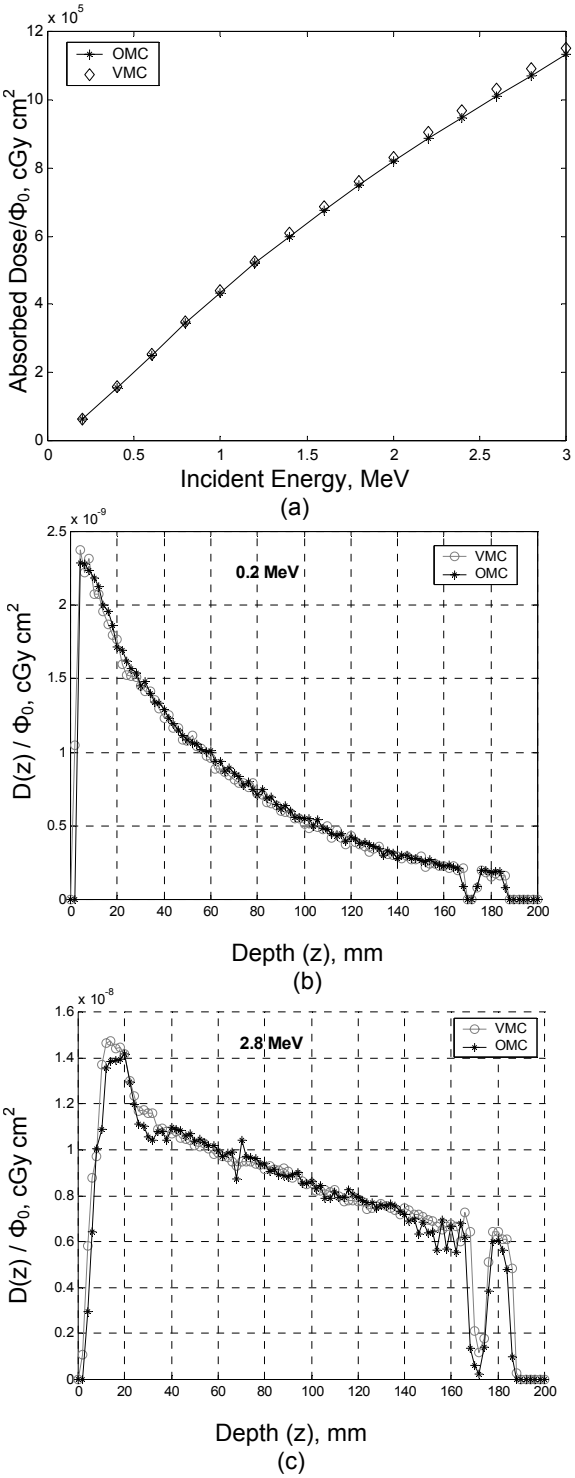


Figure 8: (a) Comparison of doses absorbed in the solid and tomographic phantoms; (b) CDD comparison for 0.2 MeV and (c) 2.8 MeV.

Irradiation was simulated at 36 positions of the gantry head in the full gantry rotation range, i.e. from 0° to 360° with discrete step of 2 degrees. A 6MV photon beam was used to obtain the simulated dose distributions. The latter were obtained using $5\times10^8$ photon histories. The beam was collimated to a $10\times10$ $cm^2$ field size, defined at the isocenter. Dose matrix voxel size was $2\times2\times2$ $mm^3$.

Figure 9 presents the comparison of simulated dose profiles through the two neck phantoms. The results show maximal discrepancies of 4% observed at the PTV plateau.

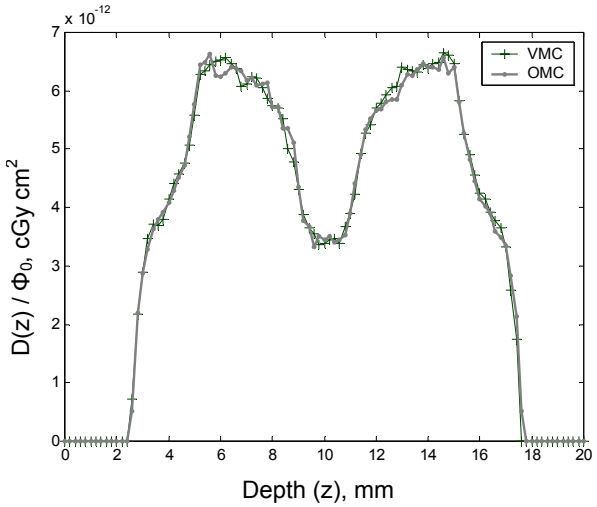


Figure 9: Dose profile comparison between data simulated through solid (OMC) and voxel-based (VMC) phantoms.

The experiments carried out with voxel-based phantoms were much more computationally expensive (about 7-8 times) than those including solid geometry phantoms. For example, in case of heterogeneous phantom and polyenergetic photon beam (experiment 2c), one of the most computationally expensive experiments, the application run in a local network, composed of 7 computers, each with the following configuration: Pentium 4.0 at 2.4 GHz and 256 MB RAM memory. With this initial setup, the dose distributions were obtained in seven days ($23\times10^7$ incident photons). For comparison, the same experiment carried out with solid geometry objects was accomplished for less than 24 hours.

## Discussion

The newly developed simulator was successfully tested to compute dose distributions obtained in various simple and complex voxel-based phantoms using monoenergetic and polyenergetic photon beams. The comparison between the two simulated CDD curves (Figure 6a) for homogeneous phantom shows an excellent match with an overall discrepancy of less than 2%. Very good coincidence between the extracted dose profiles at different depths (Figure 6b) is also observed. In case of polyenergetic beam, the comparison of the central-axis PDD between the two simulations (Figure 6c) shows an average deviation of 4%. The newly developed Monte Carlo code may therefore be stated to be successfully tested to simulate dose distributions from monoenergetic and polyenergetic photon beams in voxel-based phantoms against data produced with MCRTS using solid geometry phantoms.

The same is valid for the case of heterogeneous voxel-based absorbers. Figure 7a shows a discrepancy of less than 1% between the two simulated CD curves. Comparison of dose profiles (Figure 7b) also demonstrates satisfactory agreement between the two


ISSN: 1727-1983 

simulations. The non-uniformity of the profile curves is attributed to the small dose voxel size. Increasing the number of simulation runs will smooth the profile plateaus. A discrepancy of less than 3% is also observed between the PDD curves obtained by the two simulations (figure 7c) for heterogeneous phantom with 6 MV photon beam. The largest discrepancy is observed at the inhomogeneous boundaries, primarily due to the different mechanisms used for managing electron transport through boundaries. However, the VSM gives more precise results, since the transport through voxel-based phantom was modeled very precisely. Also, increasing the voxel size in z dimension, is expected to lead to coincidence between the curves.

The experiment involving the head tomographic phantom shows also that the VSM can calculate accurately the absorbed dose in the phantom under irradiation (Figure 8a). Differences are mostly observable at higher energies, where electron transport starts to play an important role. The chosen voxel size also was too fine, so increasing the voxel size, these differences are expected to be diminished. This difference is in process of clarification.

Similarly, observations revealed very good agreement between the two simulations of rotational radiotherapy application. A maximum deviation of less than 4% is observed in the build up region. As seen from Figure 9, the build-up regions of the dose distribution calculated in the voxel-based phantom are smoother than those in the solid geometry object. This comparison shows that VSM is a reliable tool in simulations including complex phantoms and geometries.

Simulation time, however, has been increased significantly in comparison with simulation through simple phantoms. In order to decrease the time for the simulations, we have developed a high performance local network of seven personal computers to be used routinely as instruments of evaluation of treatment plans.

**Conclusions**

This work presented the verification of additional software module used to simulate the transport of particles through complex phantoms and geometries and to calculate 3D dose distributions. Further verification is in progress examining more complex cases.

**Acknowledgments**

We thank the European Social Fund (ESF), Operational Program of Educational and Vocational Training II (EPEAEK II), and particularly the program PYTHAGORAS, for funding the above work.

**References**

[1] BRAHME A., (1997) 'The need for accurate target and dose specifications in conventional and conformal radiation therapy--an introduction' *Acta Oncol.* **36**, pp.789-792.

[2] BLIZNAKOVA K., KOLITSI Z., and PALLIKARAKIS N., (2004) 'A Monte Carlo based software tool for radiotherapy investigations' *Nucl. Instr. Meth. B* **222,** pp. 445-461.

[3] IVANOVA T., and BLIZNAKOVA K., (2004) 'Development and verification of a software module for simulation of filters in conformal radiotherapy' 4th European Symposium on Biomedical Engineering, Patras, Greece, 2004.

[4] BLIZNAKOVA K., BLIZNAKOV Z., BRAVOU V., KOLITSI Z., and PALLIKARAKIS N., (2003) 'A 3D breast software phantom for mammography simulation' *Phys. Med. Biol.* **48**, pp. 3699 – 3721.

[5] BADEA C., BULIEV I., BLIZNAKOVA K., KOLITSI Z., and PALLIKARAKIS N., (2002) 'Patient positioning verification using tomosynthetic portal tomograms', 3rd European symposium on MP/BME, Patras, Greece, 30 Aug – 1 Sep, 2002.

[6] National Library of Medicine's Visible Human Project®, http://www.nlm.nih.gov/research/visible


ISSN: 1727-1983 